

Generative Adversarial Learning of Sinkhorn Algorithm Initializations

Jonathan Geuter¹ Ingimar Tomasson² Vaios Laschos³

Abstract

The Sinkhorn algorithm is the state-of-the-art to approximate solutions of entropic optimal transport (OT) distances between discrete probability distributions. We show that meticulously training a neural network to learn initializations to the algorithm via the entropic OT dual problem can significantly speed up convergence, while maintaining desirable properties of the Sinkhorn algorithm, such as differentiability and parallelizability. We train our predictive network in an adversarial fashion using a second, generating network and a self-supervised bootstrapping loss. The predictive network is universal in the sense that it is able to generalize to any pair of distributions of fixed dimension and cost at inference, and we prove that we can make the generating network universal in the sense that it is capable of producing any pair of distributions during training. Furthermore, we show that our network can even be used as a standalone OT solver to approximate regularized transport distances to a few percent error, which makes it the first meta neural OT solver.

1. Introduction

Optimal Transport (Villani, 2009; Peyré & Cuturi, 2019) plays an increasing role in various areas in machine learning, such as domain adaptation (Courty et al., 2017), single-cell genomics (Schiebinger et al., 2019), imitation learning (Dadashi et al., 2020), imaging (Schmitz et al., 2018), dataset adaptation (Alvarez-Melis & Fusi, 2021), and signal processing (Kolouri et al., 2017). Typically, machine learning based OT solvers aim to solve a single instance of an OT problem at a time, and a new problem requires training a new solution from scratch. A meta learning approach, i.e. learning to generalize across problem instances, has

¹School of Engineering and Applied Sciences, Harvard
²Department of Mathematics, Technische Universität Berlin, Germany
³Weierstrass Institute, Berlin, Germany. Correspondence to: Jonathan Geuter <jonathan.geuter@gmx.de>.

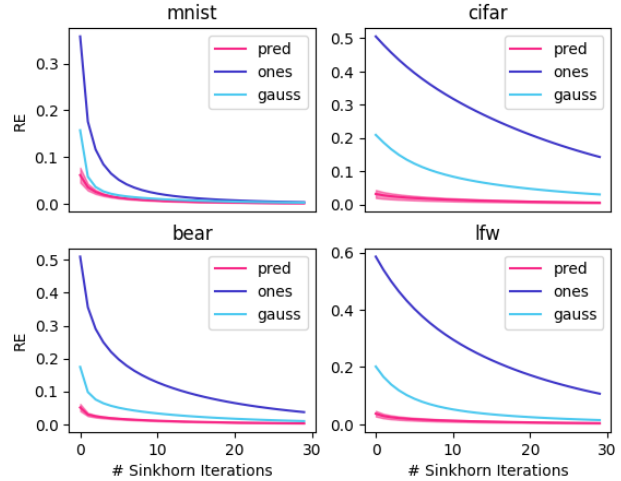


Figure 1. Relative error on the transport distance of our Sinkhorn initialization (pred), compared to the standard (ones) and a Gaussian initialization (gauss) (Thornton & Cuturi, 2022).

first been studied in (Amos et al., 2022), however only in a constrained setting for low-dimensional datasets such as MNIST. We aim to learn a *universal* neural OT solver, which can approximately solve *any* discrete, entropic OT problem of fixed dimension and cost. This makes our approach the first dataset independent meta OT solver.

To this end, our *approximator* is a neural network trained to predict a potential of the entropic OT dual problem, given two distributions as input. Training will be self-supervised in a bootstrapped fashion; at each iteration of the training algorithm we perform a few Sinkhorn iterations on the output of the approximator to generate a target potential. The crucial question is: What is the best way to generate training samples? The training dataset needs to be rich enough to allow the network to generalize to samples from any dataset during testing. We tackle this issue with a two-network approach, where a second network (the *generator*) learns to generate training samples from a Gaussian prior while the approximator learns to predict dual potentials given the generating network’s outputs. The generator, denoted by q_θ with parameters θ , is a three-layer ResNet (He et al., 2016), and we prove that we can train it in a way that makes

it universal, in the sense that it is capable of generating *any* pair of distributions; in fact, this result is proven for a very general class of ResNets. The approximator, denoted by h_ϕ with parameters ϕ , is a three-layer fully connected network. The networks will be trained in an alternating, adversarial fashion similar to a Generative Adversarial Network (Goodfellow et al., 2014; Wang et al., 2017; Creswell et al., 2018) (GAN), where the generator’s loss is negative the approximator’s loss.

While our predicted transport distances lie within a few percent relative error of the true distances, we will see that we can run a few Sinkhorn algorithm (Cuturi, 2013) iterations for even more accurate approximations, significantly speeding up convergence of the algorithm while maintaining all its desirable properties such as computational efficiency, differentiability, and parallelizability. Figure 1 shows that our predicted initializations (pred) vastly outperform both the standard initialization of a vector of ones (ones) and the Gaussian initialization (gauss) from (Thornton & Cuturi, 2022) across diverse datasets.

2. Related Work

Initializing Sinkhorn. There exists very little literature on initializing the Sinkhorn algorithm. (Thornton & Cuturi, 2022) propose using dual vectors recovered from the unregularized 1D optimal transport problem, or from closed-form transport maps in a Gaussian (mixture) setting, and were able to significantly speed up convergence. In (Amos et al., 2022), a learned approach is taken as well. They use a single network to learn potentials of the dual problem via

$$\text{loss}(\mu, \nu) = -(\langle \text{net}(\mu, \nu), \mu \rangle + \langle \text{net}(\mu, \nu)^C, \nu \rangle)$$

for a pair of input distributions (μ, ν) , where $\text{net}(\mu, \nu)^C$ denotes the C -transform (cmp. (Villani, 2009)), C being the cost matrix; i.e., they maximize the optimal transport dual, cf. section 3. This approach works well when training on low-dimensional datasets such as MNIST, and is elegant in being fully unsupervised, but is not able to generalize to out-of-distribution data, i.e. is not universal.

In section 5 we will exhibit that our method generalizes across datasets unlike (Amos et al., 2022), and provides significantly better initializations than (Thornton & Cuturi, 2022).

Learning OT Distances. Various works deal with directly learning OT distances or maps in specific settings. (Courty et al., 2018) propose learning a Wasserstein embedding in Euclidean space, which works well empirically, yet no theoretical guarantees for universal embeddability exist. Typically, neural approaches for learning OT distances aim at solving single instances of (high-dimensional) OT problems. In (Bunne et al., 2022a), transport maps between continuous input distributions conditioned on a context variable

are learned. This approach builds on Input Convex Neural Networks (Amos et al., 2017). In (Gracyk & Chen, 2022), a network is trained to learn the Wasserstein geodesic between two continuous input distributions. This approach builds upon the dynamic OT formulation (Benamou & Brenier, 2000) and was able to significantly reduce computation costs. Another interesting recent paper (Uscidda & Cuturi, 2023) suggests a universal regularizer, called the *Monge gap*, to learn OT maps and distances.

Unlike these works, we focus on *generalizing across* (lower dimensional) OT problems.

OT for Machine Learning. Apart from using machine learning to approximate optimal transport distances and maps, the reverse direction – leveraging OT to formulate new machine learning methods – has also seen a surge in popularity in recent years. Oftentimes, Wasserstein distances are used in loss functions as a generic tool to measure discrepancies between distributions, such as in the celebrated Wasserstein GAN (Arjovsky et al., 2017), multi-label learning (Frogner et al., 2015), inverse problems in physics (Engquist & Yang, 2019), or few-shot image classification to compute distances between images (Zhang et al., 2020). Another interesting application lies in the area of gradient flows, which can be approximated using the Jordan-Kinderlehrer-Otto scheme; this involves solving OT problems (Alvarez-Melis & Fusi, 2021; Alvarez-Melis et al., 2022; Bunne et al., 2022b).

Generative Modelling. In generative modelling, the goal is usually to find a parametrized distribution ρ_θ which minimizes, in some metric, the distance to a target distribution ρ_{data} . Typically, this means minimizing some functional $F(\rho_\theta) = d(\rho_\theta, \rho_{\text{data}})$, where d measures the discrepancy between the distributions, and samples from ρ_{data} are usually available. While our generator also tries to learn such a parametrized distribution ρ_θ , our approach differs from this framework in that we do not have access to a given target distribution. In fact, crucially, our target distribution *changes during training*. Another similarity can be found in our loss function, which resembles the loss function of GANs. Given samples $z \sim \rho_z$ from a (Gaussian) prior and samples $x \sim \rho_{\text{data}}$ from the target distribution, the GAN objective is

$$\min_G \max_D \mathbb{E}_{x \sim \rho_{\text{data}}} [\log D(x)] + \mathbb{E}_{z \sim \rho_z} [\log(1 - D(G(z)))] ,$$

where G is the generator and D the so-called *discriminator*, which predicts the probability that a sample came from the target distribution rather than the generator. Similarly, our two-network objective will be of the form

$$\max_{\theta} \min_{\phi} \mathbb{E}_{z \sim \rho_z} [L_H(\tau(h(q(z))), h_\phi(q_\theta(z)))] ,$$

where L_H is the *Hilbert projective metric* (section 4.3), and τ denotes a target created by running a few Sinkhorn

iterations (section 4.2); cf. section 4.4 for training details. Importantly, note that our generator aims to *maximize* the objective, while the GAN generator aims to *minimize* it.

Various kinds of generative models exist. Besides GANs, Variational Auto-Encoders (Kingma & Welling, 2014; 2019), and Diffusion Models (Sohl-Dickstein et al., 2015; Song & Ermon, 2019), a fast-growing line of work is that of Normalizing Flows (Dinh et al., 2015; Rezende & Mohamed, 2015; Ho et al., 2019; Kobyzev et al., 2021; Papamakarios et al., 2021), which are compositions of parametrized, invertible transformations pushing a (typically Gaussian) probability distribution to a target distribution. Our approach shares many common characteristics; in particular, we will see in section 4.1 how to make our generator invertible by controlling its Lipschitz constant.

3. Optimal Transport

In this section, we recall some properties of optimal transport in the discrete case. We will write vectors in bold and matrices as capital letters. By $\llbracket n \rrbracket$ we refer to the set $\{1, 2, \dots, n\}$. By $\mathbf{1}_n \in \mathbb{R}^n$ we denote the vector where all entries are equal to 1. The $n-1$ dimensional simplex in \mathbb{R}^n will be denoted by Δ^{n-1} , and all elements in the simplex with positive entries are denoted by $\Delta_{>0}^{n-1}$. In the following, let $\boldsymbol{\mu}$ and $\boldsymbol{\nu}$ be two discrete, m - resp. n -dimensional probability measures on some spaces $\mathcal{X} = \{x_1, \dots, x_m\}$ and $\mathcal{Y} = \{y_1, \dots, y_n\}$ equipped with the discrete topologies. We will oftentimes abuse notation by considering $\boldsymbol{\mu}$ and $\boldsymbol{\nu}$ to be the vectors $[\mu_1 \ \dots \ \mu_m]^\top \in \Delta^{m-1}$ resp. $[\nu_1 \ \dots \ \nu_n]^\top \in \Delta^{n-1}$.

3.1. Unregularized Optimal Transport

The discrete OT problem is defined as follows.

Problem 3.1 (Optimal Transport Problem).

$$L(\boldsymbol{\mu}, \boldsymbol{\nu}) := \min_{\Gamma \in \Pi(\boldsymbol{\mu}, \boldsymbol{\nu})} \langle C, \Gamma \rangle$$

Here, $\Pi(\boldsymbol{\mu}, \boldsymbol{\nu})$ denotes the set of all *transport plans* between $\boldsymbol{\mu}$ and $\boldsymbol{\nu}$, i.e. matrices $\Gamma \in \mathbb{R}_{\geq 0}^{m \times n}$ s.t. $\Gamma \mathbf{1}_n = \boldsymbol{\mu}$ and $\Gamma^\top \mathbf{1}_m = \boldsymbol{\nu}$. The problem has a dual formulation:

Problem 3.2 (Dual Optimal Transport Problem).

$$D(\boldsymbol{\mu}, \boldsymbol{\nu}) := \max_{\substack{\mathbf{f} \in \mathbb{R}^m, \mathbf{g} \in \mathbb{R}^n \\ \mathbf{f} + \mathbf{g} \leq C}} \langle \mathbf{f}, \boldsymbol{\mu} \rangle + \langle \mathbf{g}, \boldsymbol{\nu} \rangle$$

Here, $\mathbf{f} + \mathbf{g} \leq C$ is to be understood as $f_i + g_j \leq C_{ij}$ for all $i \in \llbracket m \rrbracket, j \in \llbracket n \rrbracket$. In the special case where $\mathcal{X} = \mathcal{Y}$ and C corresponds to a metric, i.e. $C_{ij} = d(x_i, y_j)$, the Wasserstein distance of order p between $\boldsymbol{\mu}$ and $\boldsymbol{\nu}$ for $p \in$

$[1, \infty)$ is defined as

$$W_p(\boldsymbol{\mu}, \boldsymbol{\nu}) = \left(\min_{\gamma \in \Pi(\boldsymbol{\mu}, \boldsymbol{\nu})} \sum_{i,j} C_{ij}^p \gamma_{ij} \right)^{\frac{1}{p}},$$

which is a distance in the space of probability measures (Villani, 2009).

3.2. Entropic Optimal Transport

A common regularization of the problem consists of adding an entropic regularizer.

Problem 3.3 (Entropic Optimal Transport Problem). For $\varepsilon > 0$, the entropic optimal transport problem is defined as:

$$L^\varepsilon(\boldsymbol{\mu}, \boldsymbol{\nu}) := \min_{\Gamma_\varepsilon \in \Pi(\boldsymbol{\mu}, \boldsymbol{\nu})} \langle C, \Gamma_\varepsilon \rangle - \varepsilon H(\Gamma_\varepsilon),$$

where $H(\Gamma_\varepsilon) := -\sum_{i=1}^m \sum_{j=1}^n \Gamma_{ij}^\varepsilon (\log \Gamma_{ij}^\varepsilon - 1)$ is the entropy of the transport plan.¹

Note that this is identical to the regular optimal transport problem, except that the regular one does not contain the regularization term $-\varepsilon H(\Gamma)$. As the objective in Problem 3.3 is ε -strongly convex, the problem admits a unique solution (Peyré & Cuturi, 2019). Again, this problem admits a dual formulation:

Problem 3.4 (Entropic Dual Problem).

$$D^\varepsilon(\boldsymbol{\mu}, \boldsymbol{\nu}) := \max_{\mathbf{f}_\varepsilon \in \mathbb{R}^m, \mathbf{g}_\varepsilon \in \mathbb{R}^n} \langle \mathbf{f}_\varepsilon, \boldsymbol{\mu} \rangle + \langle \mathbf{g}_\varepsilon, \boldsymbol{\nu} \rangle - \varepsilon \left\langle e^{\mathbf{f}_\varepsilon/\varepsilon}, K e^{\mathbf{g}_\varepsilon/\varepsilon} \right\rangle,$$

where $K := \exp(-C/\varepsilon)$ is the *Gibbs kernel*. As before, without the regularization term $-\varepsilon \langle e^{\mathbf{f}_\varepsilon/\varepsilon}, K e^{\mathbf{g}_\varepsilon/\varepsilon} \rangle$, this equals the regular optimal transport dual; note, however, that the unregularized dual is subject to the constraint $\mathbf{f} + \mathbf{g} \leq C$. The following proposition holds (see, e.g., (Peyré & Cuturi, 2019)).

Proposition 3.5. *The unique solution of Problem 3.3 is given by*

$$\Gamma_\varepsilon = \text{diag}(\mathbf{u}) K \text{diag}(\mathbf{v})$$

for two positive scaling vectors \mathbf{u} and \mathbf{v} unique up to a scaling constant (i.e. $\lambda \mathbf{u}, \frac{1}{\lambda} \mathbf{v}$ for $\lambda > 0$). Furthermore, (\mathbf{u}, \mathbf{v}) are linked to a solution $(\mathbf{f}_\varepsilon, \mathbf{g}_\varepsilon)$ of Problem 3.4 via

$$(\mathbf{u}, \mathbf{v}) = (\exp(\mathbf{f}_\varepsilon/\varepsilon), \exp(\mathbf{g}_\varepsilon/\varepsilon)).$$

From here on out, we will always use \mathbf{f} and \mathbf{g} to denote the vectors from the dual problem, and \mathbf{u} and \mathbf{v} to denote the respective vectors in log-space.

¹For entries $\Gamma_{ij}^\varepsilon = 0$, we use the convention $0 \log 0 = 0$, as $x \log x \xrightarrow{x \rightarrow 0} 0$.

3.3. Sinkhorn Algorithm Initializations

The Sinkhorn algorithm – see Algorithm 1 – is an iterative procedure based on the original work of Sinkhorn and Knopp (Sinkhorn & Knopp, 1967). It was first applied to the optimal transport setting in the seminal work *Sinkhorn distances: lightspeed computation of optimal transport* (Cuturi, 2013).

Algorithm 1 Sinkhorn Algorithm

```

1: in  $C \in \mathbb{R}^{m \times n}$ ,  $\varepsilon > 0$ ,  $\mu \in \Delta_{>0}^{m-1}$ ,  $\nu \in \Delta_{>0}^{n-1}$ 
2: initialize  $v^0$  (e.g.  $v^0 \leftarrow 1_n$ ),  $l \leftarrow 0$ ,  $K \leftarrow \exp(-C/\varepsilon)$ 
3: repeat
4:    $u^{l+1} \leftarrow \mu ./ K v^l$ 
5:    $v^{l+1} \leftarrow \nu ./ K^\top u^{l+1}$ 
6:    $l \leftarrow l + 1$ 
7: until stopping criterion is met
8:  $\Gamma \leftarrow \text{diag}(u^l) K \text{diag}(v^l)$ 
9:  $\gamma \leftarrow \langle C, \Gamma \rangle$ 
10: out  $\Gamma, \gamma$ 
    
```

In the algorithm, $./$ is to be understood as element-wise division. Note that the algorithm requires both input distributions to be positive everywhere to prevent division by zero. As Sinkhorn and Knopp showed in their original work, the iterates u^l and v^l from the algorithm converge to the vectors u and v from Proposition 3.5. This implies that the transport plan and distance generated by the algorithm converge towards the minimizer and minimum value in Problem 3.3. By Proposition 3.5, we know that $v = \exp(g_\varepsilon/\varepsilon)$ for a solution g_ε of the regularized dual. Hence, if we can train a neural network to approximate v from Proposition 3.5 for any pair of distributions (μ, ν) of fixed dimension n for a fixed regularizer ε , this will let us solve the regularized OT problem.² Since computations in the log domain tend to be more computationally stable (Peyré & Cuturi, 2019), we will instead let the network learn $\log(v) =: g^*$, where we add a superscript $'*$ to denote the true underlying potential, and refer to our network’s approximation of it as g .³ Then, one can use this approximation as an initialization for the Sinkhorn algorithm via $v^0 = \exp(g)$. Note that the solution to the entropic dual 3.4 is not unique, as can be seen from proposition 3.5. How we deal with this fact in learning solutions will be explained in section 4.3. When endowing $\mathbb{R}^m \times \mathbb{R}^n$ with the equivalence relation $(u_1, v_1) \sim (u_2, v_2) \Leftrightarrow \exists \lambda > 0 : (u_1, v_1) = (\lambda u_2, \frac{1}{\lambda} v_2)$ (i.e. the equivalence relation that accounts for the non-uniqueness of the solution of the dual problem 3.4), the map $(\mu, \nu) \mapsto v$, mapping two measures to the associated

²While we will choose μ and ν to have the same dimension n for practical reasons, as most datasets tend to have constant dimension, our framework is not constrained to this setting.

³Hence, what we will call g^* from now on for ease of notation is equal to $g_\varepsilon/\varepsilon$.

dual potential in the quotient space, is Lipschitz continuous (Carlier et al., 2022), which supports its learnability by a neural network.

4. Learning Initializations

In this section, we describe our algorithm and theoretically support it. Details about hyperparameter and architecture choices can be found in Appendix B. All code is available at https://github.com/ingitom99/learn_sink.

4.1. Generator

The generator is a ResNet-like network, where inputs z come from an l -dimensional Gaussian prior, $z \sim \rho_z = \mathcal{N}(0, I)$, and the output is given by

$$(\mu, \nu) = q_\theta(z) = \text{Renorm}[\text{ReLU}(\text{net}_\theta(z) + \lambda T(z)) + c],$$

where net_θ is a trainable neural network, T is a skip connection that interpolates its input to match the generator’s output dimension, and λ is a constant controlling the impact of the skip connection. We add a small constant c to make sure that the output is non-zero everywhere, which is a requirement of the Sinkhorn algorithm. *Renorm* denotes renormalizing to two probability measures. The generator is universal in the following sense:

Theorem 4.1. *Let $0 < \lambda < 1$ and $q : \mathbb{R}^k \rightarrow \mathbb{R}^k$ be defined via*

$$q(z) = \text{ReLU}(\lambda z + \text{net}_\theta(z)),$$

where $z \sim \rho_z = \mathcal{N}(0, I)$, and where $\text{net}_\theta : \mathbb{R}^k \rightarrow \mathbb{R}^k$ is Lipschitz continuous with $\text{Lip}(\text{net}_\theta) = L < \lambda$. Then q is Lipschitz continuous with $\text{Lip}(q) < L + \lambda$, and for any $x \in \mathbb{R}_{\geq 0}^k$ it holds

$$\rho_{q\#\rho_z}(x) \geq \frac{1}{(L + \lambda)^k} \mathcal{N}(q^{-1}(x) | 0, I).$$

In other words, q has positive density at any non-negative $x \in \mathbb{R}_{\geq 0}^k$.

The proof can be found in Appendix A.

Remark 4.2. This theorem can easily be extended to compositions of such functions q , as compositions of Lipschitz functions are again Lipschitz.

Note that Theorem 4.1 is not directly applicable to our setting for a few reasons: First, we add a small constant c to the generator’s output. This constant ensures that all training samples are positive everywhere, and vastly improves learning speed as it ensures that all inputs are active. However, this is not restrictive of the problem, as the Sinkhorn algorithm requires inputs to be positive anyways. Second, in Theorem 4.1 both in- and outputs to q have the same

dimension. This could be achieved in our setting by choosing the input dimension equal to the output dimension, i.e. T equal to the identity. However, in practice, using lower-dimensional inputs achieves significantly better results. This can be argued for by the manifold hypothesis (Fefferman et al., 2016), i.e. the fact that typically, datasets live on low-dimensional manifolds embedded in high-dimensional spaces. Depending on the application, i.e. the expected target dataset dimension, the dimension of the input can be adjusted accordingly. Finally, note that the theorem assumes that net_θ is Lipschitz continuous with Lipschitz constant $L < \lambda$, where λ is the scaling factor of the skip connection. We do not enforce this constraint, as not doing so yields empirically better results. Still, theorem 4.1 goes to show that our algorithm’s performance is not bottlenecked by the generator’s inability to generalize. Details on how one could bound the Lipschitz constant can be found in Appendix B. We note that a bound on the Lipschitz constant is not necessary for invertibility of ResNets; other approaches have been suggested in the literature, e.g. through the lens of ODEs (Chang et al., 2017) or by partitioning input dimensions (Jacobsen et al., 2018). It is also possible to directly divide by the Lipschitz constant of each layer (Serrurier et al., 2023); these approaches could be studied in future research.

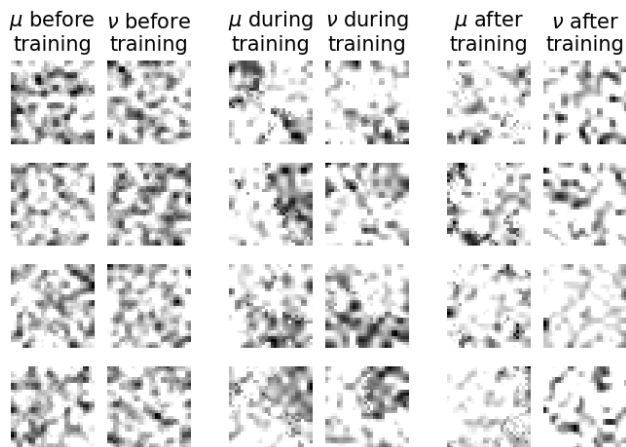


Figure 2. Generated pairs of training samples (darker=more mass).

Figure 2 shows pairs of training samples generated by the generator over the course of training. One can see that at different stages of training, it can be beneficial to place mass either at close by locations in μ and ν (here, during training), as well as at distinct locations (here, at the end of training). Also, there seems to be a trend towards greater sparsity over the course of training.

4.2. Targets

We want our approximator to learn dual potentials \mathbf{g}^* . Hence, in order to compute targets during training, for each

training sample (μ, ν) one could compute the respective potential \mathbf{g}^* using the Sinkhorn algorithm. This approach, however, is computationally very expensive and dramatically slows down training. Hence, we instead employ a bootstrapped version of the idea: given the approximator’s output \mathbf{g} for a training sample, we compute a target

$$\mathbf{g}_\tau := \tau(\mathbf{g}) := \log \text{k-SH}(\exp(\mathbf{g})),$$

where k-SH denotes running k Sinkhorn iterations for a very small number k (as $k \rightarrow \infty$, one would recover computing exact targets instead). This approach allows for efficient target computation, and in the following section we will see that this choice of targets provably leads to learning the true potentials when the loss is minimized.

4.3. Loss Function

This section introduces the approximator’s loss – how the generator learns using this loss is explained in the following section 4.4. We use the Hilbert projective metric as a loss, as it guarantees geometric convergence of the Sinkhorn algorithm from a theoretical point of view (Franklin & Lorenz, 1989), and works well empirically. The Hilbert projective metric between two vectors $\mathbf{u}, \mathbf{v} \in \mathbb{R}_+^n$ is defined as

$$d_H(\mathbf{u}, \mathbf{v}) := \max_i [\log(u_i) - \log(v_i)] - \min_i [\log(u_i) - \log(v_i)].$$

Since our network is operating in log space, we define (using \mathbf{f} and \mathbf{g} for consistency, as these vectors lie in log space):

$$L_H(\mathbf{f}, \mathbf{g}) := \max_i [f_i - g_i] - \min_i [f_i - g_i].$$

Note that this loss is invariant under translating the vectors by constants, which corresponds to the solution to the optimal transport dual problem 3.4 being invariant under constant translations. In other words, this enables the network to learn the best intrinsic representation of solutions to the dual, without constraining *which* dual solution we want to learn for a given sample.

Consequently, for a sample (μ, ν) , our approximator’s loss is given by

$$\text{loss}(\mu, \nu) = L_H(\tau(h(\mu, \nu)), h_\phi(\mu, \nu)),$$

where h does not have a subscript for its parameters in the first term of L_H as this term denotes the target, which we do not backpropagate through. The following proposition formalizes why learning with this bootstrapping loss works.

Proposition 4.3. *For a data sample (μ, ν) , let $\mathbf{g}^* = \mathbf{g}_\varepsilon/\varepsilon$ be a potential solving the dual problem, $\mathbf{g} = h(\mu, \nu)$ the approximator’s prediction, and $\mathbf{g}_\tau = \log \text{k-SH}(\exp(\mathbf{g}))$ the target. Then*

$$L_H(\mathbf{g}, \mathbf{g}^*) \leq c(K, k)L_H(\mathbf{g}_\tau, \mathbf{g})$$

for some constant $c(K, k) > 1$ depending only on the Gibb’s kernel K and the integer k .

The proposition shows that learning to minimize loss $(\mu, \nu) = L_H(\mathbf{g}_\tau, \mathbf{g})$ implies learning to minimize the distance $L_H(\mathbf{g}, \mathbf{g}^*)$ between the approximator’s prediction and the ground truth. A proof can be found in appendix A.

4.4. Training

Our approximator tries to minimize the loss introduced in the previous section. For training, the samples (μ, ν) will be generated by the generator, and the generator will try to maximize the same loss function simultaneously in order to produce samples which the approximator has not learned yet. Consequently, our training objective reads

$$\max_{\theta} \min_{\phi} \mathbb{E}_{z \sim \rho_z} [L_H(\tau(h(q(z))), h_{\phi}(q_{\theta}(z)))] ,$$

where h and q again do not have subscripts for their parameters in the first term of L_H as we do not backpropagate through this term. The training algorithm can be seen in Algorithm 2.

Algorithm 2 Training Algorithm

- 1: **in** cost $C \in \mathbb{R}^{n \times n}$, reg parameter ε , prior ρ_z , learning rates $\{\alpha_i\}_i, \{\beta_i\}_i$
 - 2: **for** $i = 1, 2, \dots, T$ **do**
 - 3: $z \leftarrow \text{sample}(\rho_z)$
 - 4: $(\mu, \nu) \leftarrow q_{\theta}(z)$
 - 5: $\mathbf{g}_{\phi} \leftarrow h_{\phi}(\mu, \nu)$
 - 6: $\mathbf{g}_{\tau} \leftarrow \tau(\mathbf{g}_{\phi})$
 - 7: $\phi \leftarrow \phi - \alpha_i \nabla_{\phi} L_H(\mathbf{g}_{\tau}, \mathbf{g}_{\phi})$
 - 8: $\mathbf{g}_{\theta} \leftarrow h_{\phi}(\mu, \nu)$
 - 9: $\mathbf{g}_{\tau} \leftarrow \tau(\mathbf{g}_{\theta})$
 - 10: $\theta \leftarrow \theta + \beta_i \nabla_{\theta} L_H(\mathbf{g}_{\tau}, \mathbf{g}_{\theta})$
 - 11: **end for**
-

De facto, z in Algorithm 2 will contain a batch of samples and all computations will be batched accordingly. Note that vectors \mathbf{g} with subscripts θ or ϕ are backpropagated through with respect to these parameters, and a subscript τ denotes target vectors, which we do not backpropagate through. C and ε are implicitly used in the function τ .

5. Experiments

In all experiments in this section we are averaging over a batch of 500 samples from each test dataset. In Figures 1, 6, 7, and 8, we plot the 95% confidence intervals alongside the mean values of 5 independent training runs; however, oftentimes, the confidence intervals are too narrow to be visible.

5.1. Test Sets

We test the network on four different image datasets: MNIST, the teddy bear class from the [Google Quick](#),

[Draw!](#) dataset, ‘Labelled Faces in the Wild’ (LFW), and a grayscale version of CIFAR10. All of these datasets are 28×28 –dimensional. Figure 3 shows the test datasets (with coloring for some of them inverted for better visualization). The datasets range from very low-dimensional, like MNIST, to rather high-dimensional, like CIFAR10, hence providing a good sense of generalizability of the initialization.

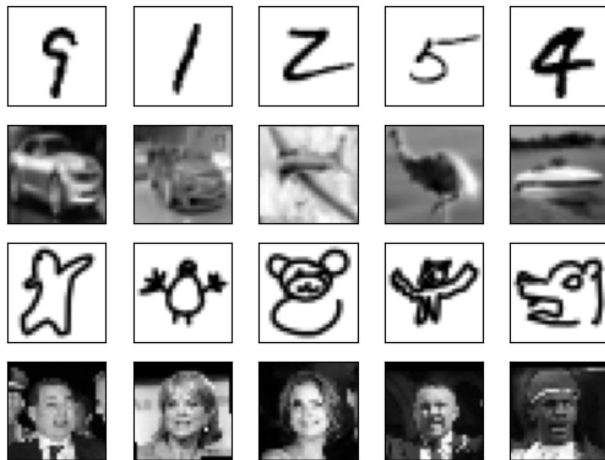


Figure 3. Test datasets ‘MNIST’, ‘CIFAR’, ‘teddies’, and ‘LFW’.

5.2. Performance Metrics

To test the quality of predictions of the approximator, we use two key metrics: Firstly, the relative error (RE) against the entropic transport distance d_{\star} (i.e the minimal objective of Problem 3.3)

$$\frac{|d^{(l)} - d_{\star}|}{|d_{\star}|},$$

where $d^{(l)}$ denotes the Sinkhorn distance after l iterations (i.e. the transport distance we get from initializing the Sinkhorn algorithm with our prediction and running it for l iterations); secondly, the marginal constraint violation (MCV), which is oftentimes used as a stopping criterion for the Sinkhorn algorithm in practice when one does not have access to the true transport distances. The MCV measures how far the transport plan $\Gamma^{(l)}$ computed by the Sinkhorn algorithm after l iterations is from fulfilling the marginal constraints $\mathbf{1}_m^{\top} \Gamma^{(l)} = \nu^{\top}$ and $\Gamma^{(l)} \mathbf{1}_n = \mu$. Different flavours to measure the MCV exist; we use

$$\frac{(\|\mathbf{1}_m^{\top} \Gamma^{(l)} - \nu^{\top}\|_1) + (\|\Gamma^{(l)} \mathbf{1}_n - \mu\|_1)}{2}.$$

5.3. Initialization Performance

We compare the Sinkhorn algorithm’s convergence for our learned initialization to the default one ($\mathbf{1}_{28} \in \mathbb{R}^{28}$) and the

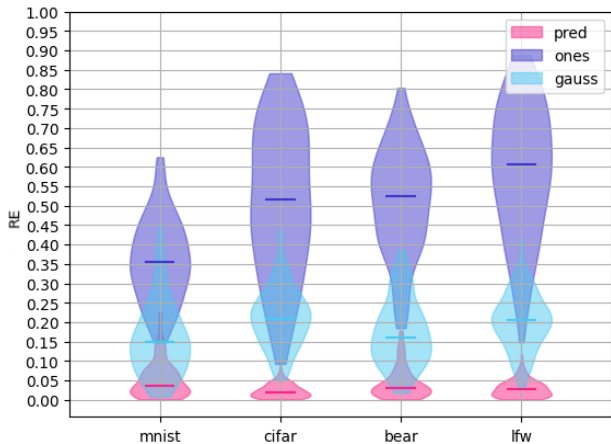


Figure 4. Relative errors on the transport distances after a single Sinkhorn iteration on our initialization ('pred'), the default initialization ('ones'), and the Gaussian initialization ('gauss').

Gaussian initialization from (Thornton & Cuturi, 2022), which is based on closed-form solutions for Gaussian distributions. We do not compare to (Amos et al., 2022), as their approach is inherently dataset dependent and breaks down when testing on out-of-distribution data, whereas the Gaussian initialization from (Thornton & Cuturi, 2022) and our learned initialization are universally applicable. The network is trained on 20,000,000 unique training samples from the generator and training takes approximately only 40 minutes on a NVIDIA V100 Tensor Core GPU with 16 GB.

The violin plots in Figure 4 and 5 show the relative error on the transport distance and the marginal constraint violation after a single Sinkhorn iteration (which we need in order to compute the second potential from the first)⁴ with the darker line in each violin representing the median of the samples from each dataset. We observe that our approximator's prediction (pred) achieves median relative errors of less than 0.05 on all of the datasets, which is an order of magnitude better than the vector of ones initialization (ones) and significantly better than the Gaussian initialization (gauss). We see similar results for the MCV. Notably, our initialization also has vastly reduced variance in accuracy, hence allowing for more robust initializations. In Figure 1 (section 1) and Figure 6 we visualize the accuracy of the Sinkhorn algorithm in terms of relative error on the transport distance and MCV over 30 iterations.

Tables 1 and 2 show the average number of Sinkhorn iterations needed to achieve 0.01 relative error on the transport distance and 0.01 MCV, resp.

⁴We can compute u from v via $u = \mu/Kv$; this identity holds in the limit of the Sinkhorn algorithm, and corresponds to the fact that the potentials of the entropic dual problem are linked via being the so-called C -transform of one another (cf. (Villani, 2009)).

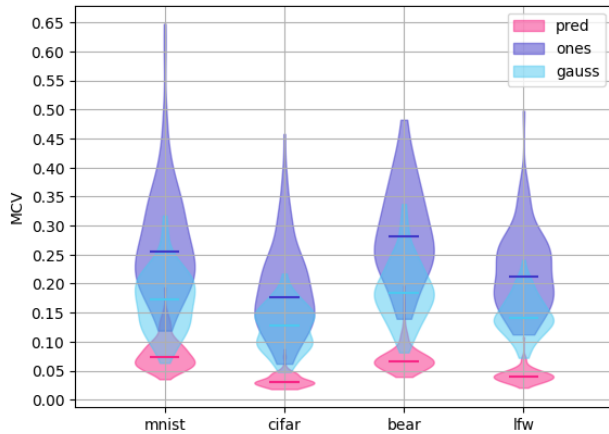


Figure 5. Marginal constraint violations after a single Sinkhorn iteration.

	PRED (OURS)	ONES	GAUSS
MNIST	6 ± 5	15 ± 10	9 ± 11
CIFAR	8 ± 17	78 ± 23	46 ± 23
LFW	8 ± 14	65 ± 19	31 ± 18
BEAR	9 ± 8	44 ± 18	22 ± 13

Table 1. Mean number of iterations needed to achieve 0.01 relative error on the OT distance (with std. deviation, rounded to integers).

	PRED (OURS)	ONES	GAUSS
MNIST	7 ± 3	13 ± 6	9 ± 5
CIFAR	3 ± 2	47 ± 15	17 ± 9
LFW	4 ± 3	41 ± 12	14 ± 4
BEAR	7 ± 3	31 ± 11	13 ± 8

Table 2. Mean number of iterations needed to achieve 0.01 MCV (with std. deviation, rounded to integers).

In Figure 7 we compare the accuracy of the approximator to that of another approximator trained on the random noise used as the input to the generator during training (upsampled to match the dimension); i.e., this one is trained without a generator. We observe that the approximator trained in conjunction with a generator achieves better performance, particularly on higher-dimensional datasets, showing that the generator is beneficial in training the approximator.

To illustrate that our approach is also efficient in terms of computation time, Figure 8 shows relative errors on the transport distance with respect to computation time. Comparing this to Figure 1, we see that the time needed to compute the initialization is negligible compared to the time needed to run Sinkhorn iterations.

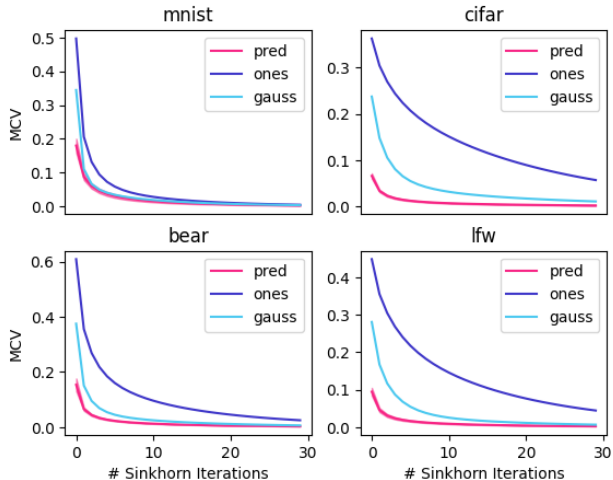


Figure 6. Marginal constraint violations over Sinkhorn iterations.

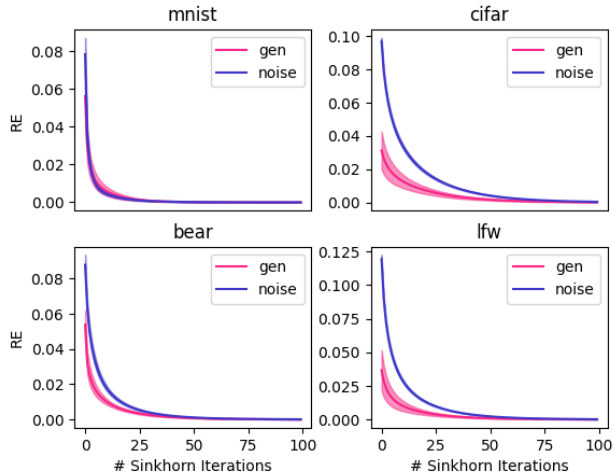


Figure 7. Comparison of relative errors on the transport distance over Sinkhorn iterations for an approximator trained on random noise ('noise') versus training with the generator ('gen').

6. Discussion

We demonstrated how to learn universal initializations to the Sinkhorn algorithm using a two-network approach, where one network is used to generate training samples for the second network. Both networks are trained in an adversarial manner similar to GANs. We proved that our generating network is universal in that it can produce any pair of distributions as training data (although we do not enforce this in practice). The networks train in a self-supervised, bootstrapped fashion, where targets are created by running a small number of Sinkhorn iterations on the prediction. We proved that learning to minimize a loss on such targets implies minimizing the loss on the true, underlying potentials. When comparing the relative errors on the entropic transport distance and marginal constraint violation of the Sinkhorn algorithm for its default initialization, a Gaussian initialization as in (Thornton & Cuturi, 2022), and our approximator’s initialization, the approximator significantly outperforms the other methods on all test datasets, showing that it can generalize to before unseen datasets. Furthermore, we demonstrate that the approximator can be used as a standalone, universal entropic OT solver, as it achieves consistently low (on average 5%) relative error on the transport distance when running a single Sinkhorn iteration on its output. To our knowledge, this makes it the first meta neural OT solver. The network is easy and fast to train, and empirically not sensitive to hyperparameters. At inference time, the computation time needed to compute the initialization is negligible compared to the time needed by the Sinkhorn algorithm. We note that our setting is fairly low-dimensional, and scaling to higher dimensions would be an important line of future research.

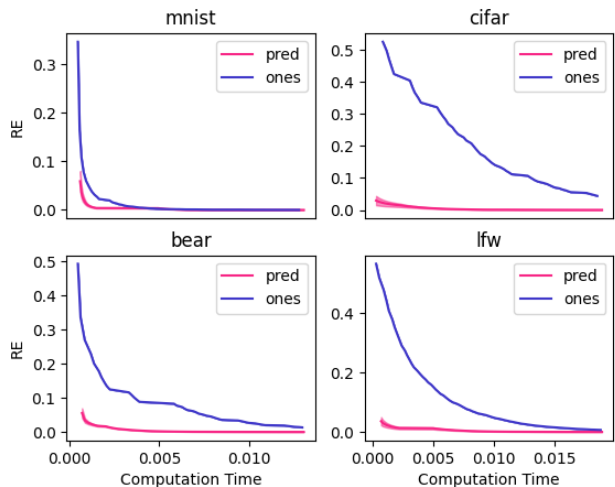


Figure 8. Comparison of relative errors on the transport distance over computation time in seconds.

Impact Statement

This paper presents work whose goal is to advance the field of Machine Learning. There are many potential societal consequences of our work as optimal transport has a vast range of applications, but none of these we feel must be specifically highlighted here.

Acknowledgements

We would like to thank Paul Hagemann for very insightful discussions, particularly regarding the generator.

References

- Alvarez-Melis, D. and Fusi, N. Dataset Dynamics via Gradient Flows in Probability Space. In Meila, M. and Zhang, T. (eds.), *Proceedings of the 38th International Conference on Machine Learning*, volume 139 of *Proceedings of Machine Learning Research*, pp. 219–230. PMLR, 18–24 Jul 2021. URL <https://proceedings.mlr.press/v139/alvarez-melis21a.html>.
- Alvarez-Melis, D., Schiff, Y., and Mroueh, Y. Optimizing Functionals on the Space of Probabilities with Input Convex Neural Networks. *Transactions on Machine Learning Research*, 2022. URL <https://openreview.net/forum?id=dpOYN7o8Jm>.
- Amos, B., Xu, L., and Kolter, J. Z. Input Convex Neural Networks. In Precup, D. and Teh, Y. W. (eds.), *Proceedings of the 34th International Conference on Machine Learning*, volume 70 of *Proceedings of Machine Learning Research*, pp. 146–155. PMLR, 06–11 Aug 2017. URL <https://proceedings.mlr.press/v70/amos17b.html>.
- Amos, B., Cohen, S., Luise, G., and Redko, I. Meta Optimal Transport, 2022. URL <https://arxiv.org/abs/2206.05262>.
- Arjovsky, M., Chintala, S., and Bottou, L. Wasserstein Generative Adversarial Networks. In Precup, D. and Teh, Y. W. (eds.), *Proceedings of the 34th International Conference on Machine Learning*, volume 70 of *Proceedings of Machine Learning Research*, pp. 214–223. PMLR, 06–11 Aug 2017. URL <https://proceedings.mlr.press/v70/arjovsky17a.html>.
- Behrmann, J., Grathwohl, W., Chen, R. T. Q., Duvenaud, D., and Jacobsen, J.-H. Invertible Residual Networks. *Proceedings of the International Conference on Machine Learning*, 2019. doi: 10.48550/ARXIV.1811.00995. URL <https://arxiv.org/abs/1811.00995>.
- Benamou, J.-D. and Brenier, Y. A computational fluid mechanics solution to the Monge-Kantorovich mass transfer problem. *Numerische Mathematik*, 84:375–393, 2000.
- Bunne, C., Krause, A., and Cuturi, M. Supervised Training of Conditional Monge Maps, 2022a. URL <https://arxiv.org/abs/2206.14262>.
- Bunne, C., Papaxanthos, L., Krause, A., and Cuturi, M. Proximal Optimal Transport Modeling of Population Dynamics. In *Proceedings of The 25th International Conference on Artificial Intelligence and Statistics*, volume 151 of *Proceedings of Machine Learning Research*, pp. 6511–6528. PMLR, 28–30 Mar 2022b. URL <https://proceedings.mlr.press/v151/bunne22a.html>.
- Carlier, G., Chizat, L., and Laborde, M. Lipschitz continuity of the schrödinger map in entropic optimal transport, 2022.
- Chang, B., Meng, L., Haber, E., Ruthotto, L., Begert, D., and Holtham, E. Reversible architectures for arbitrarily deep residual neural networks, 2017.
- Courty, N., Flamary, R., Habrard, A., and Rakotomamonjy, A. Joint distribution optimal transportation for domain adaptation. In *Advances in Neural Information Processing Systems*, volume 30, 2017. URL <https://proceedings.neurips.cc/paper/2017/file/0070d23b06b1486a538c0eaa45dd167a-Paper.pdf>.
- Courty, N., Flamary, R., and Ducoffe, M. Learning Wasserstein Embeddings. In *ICLR 2018 - 6th International Conference on Learning Representations*, pp. 1–13, Vancouver, Canada, April 2018. URL <https://hal.inria.fr/hal-01956306>.
- Creswell, A., White, T., Dumoulin, V., Arulkumaran, K., Sengupta, B., and Bharath, A. A. Generative Adversarial Networks: An Overview. *IEEE Signal Processing Magazine*, 35(1):53–65, jan 2018. doi: 10.1109/msp.2017.2765202. URL <https://doi.org/10.1109%2Fmsp.2017.2765202>.
- Cuturi, M. Sinkhorn Distances: Lightspeed Computation of Optimal Transport. In Burges, C., Bottou, L., Welling, M., Ghahramani, Z., and Weinberger, K. (eds.), *Advances in Neural Information Processing Systems*, volume 26. Curran Associates, Inc., 2013. URL <https://proceedings.neurips.cc/paper/2013/file/af21d0c97db2e27e13572cbf59eb343d-Paper.pdf>.
- Dadashi, R., Hussenot, L., Geist, M., and Pietquin, O. Primal Wasserstein Imitation Learning, 2020. URL <https://arxiv.org/abs/2006.04678>.
- Dinh, L., Krueger, D., and Bengio, Y. NICE: Non-linear Independent Components Estimation. In *ICLR Workshop*, 2015.
- Engquist, B. and Yang, Y. Seismic imaging and optimal transport. *Communications in Information and Systems*, 19(2):95–145, 2019. URL <https://www.intlpress.com/site/pub/pages/journals/items/cis/content/vols/0019/0002/a001/index.php>.
- Fefferman, C., Mitter, S., and Narayanan, H. Testing the manifold hypothesis. *Journal of the American Mathematical Society*, 29(4):983–1049, 2016.

- URL <https://www.ams.org/journals/jams/2016-29-04/S0894-0347-2016-00852-4/>.
- Franklin, J. and Lorenz, J. On the scaling of multidimensional matrices. *Linear Algebra and its Applications*, 114-115:717–735, mar-apr 1989. URL [https://doi.org/10.1016/0024-3795\(89\)90490-4](https://doi.org/10.1016/0024-3795(89)90490-4).
- Frogner, C., Zhang, C., Mobahi, H., Araya, M., and Poggio, T. A. Learning with a Wasserstein Loss. In *Advances in Neural Information Processing Systems*, volume 28. Curran Associates, Inc., 2015. URL <https://proceedings.neurips.cc/paper/2015/file/a9eb812238f753132652ae09963a05e9-Paper.pdf>.
- Goodfellow, I., Pouget-Abadie, J., Mirza, M., Xu, B., Warde-Farley, D., Ozair, S., Courville, A., and Bengio, Y. Generative Adversarial Nets. In Ghahramani, Z., Welling, M., Cortes, C., Lawrence, N., and Weinberger, K. (eds.), *Advances in Neural Information Processing Systems*, volume 27. Curran Associates, Inc., 2014. URL <https://proceedings.neurips.cc/paper/2014/file/5ca3e9b122f61f8f06494c97b1afccf3-Paper.pdf>.
- Gouk, H., Frank, E., Pfahringer, B., and Cree, M. J. Regularisation of neural networks by enforcing lipschitz continuity, 2020.
- Gracyk, A. and Chen, X. GeONet: a neural operator for learning the Wasserstein geodesic, 2022. URL <https://arxiv.org/abs/2209.14440>.
- He, K., Zhang, X., Ren, S., and Sun, J. Deep Residual Learning for Image Recognition. In *2016 IEEE Conference on Computer Vision and Pattern Recognition (CVPR)*, pp. 770–778, 2016. doi: 10.1109/CVPR.2016.90.
- Ho, J., Chen, X., Srinivas, A., Duan, Y., and Abbeel, P. Flow++: Improving Flow-Based Generative Models with Variational Dequantization and Architecture Design. In Chaudhuri, K. and Salakhutdinov, R. (eds.), *Proceedings of the 36th International Conference on Machine Learning*, volume 97 of *Proceedings of Machine Learning Research*, pp. 2722–2730. PMLR, 09–15 Jun 2019. URL <https://proceedings.mlr.press/v97/hol19a.html>.
- Jacobsen, J.-H., Smeulders, A., and Oyallon, E. i-revnet: Deep invertible networks, 2018.
- Kingma, D. P. and Welling, M. Auto-Encoding Variational Bayes. In *Proceedings of the 2nd International Conference on Learning Representations*, 2014. doi: 10.48550/ARXIV.1312.6114. URL <https://arxiv.org/abs/1312.6114>.
- Kingma, D. P. and Welling, M. An Introduction to Variational Autoencoders. *Foundations and Trends in Machine Learning*, 12(4):307–392, 2019.
- Kobyzev, I., Prince, S. J., and Brubaker, M. A. Normalizing Flows: An Introduction and Review of Current Methods. *IEEE Transactions on Pattern Analysis and Machine Intelligence*, 43(11):3964–3979, 2021. doi: 10.1109/TPAMI.2020.2992934.
- Kolouri, S., Park, S. R., Thorpe, M., Slepcev, D., and Rohde, G. K. Optimal Mass Transport: Signal processing and machine-learning applications. *IEEE Signal Processing Magazine*, 34(4):43–59, 2017. doi: 10.1109/MSP.2017.2695801.
- Papamakarios, G., Nalisnick, E., Rezende, D. J., Mohamed, S., and Lakshminarayanan, B. Normalizing Flows for Probabilistic Modeling and Inference. *Journal of Machine Learning Research*, 22(57):1–64, 2021. URL <http://jmlr.org/papers/v22/19-1028.html>.
- Peyré, G. and Cuturi, M. Computational Optimal Transport: With Applications to Data Science. *Foundations and Trends® in Machine Learning*, 11(5-6):355–607, 2019. ISSN 1935-8237. doi: 10.1561/22000000073. URL <http://dx.doi.org/10.1561/22000000073>.
- Rezende, D. and Mohamed, S. Variational inference with normalizing flows. In Bach, F. and Blei, D. (eds.), *Proceedings of the 32nd International Conference on Machine Learning*, volume 37 of *Proceedings of Machine Learning Research*, pp. 1530–1538, Lille, France, 07–09 Jul 2015. PMLR. URL <https://proceedings.mlr.press/v37/rezende15.html>.
- Schiebinger, G., Shu, J., Tabaka, M., Cleary, B., Subramanian, V., Solomon, A., Gould, J., Liu, S., Lin, S., Berube, P., Lee, L., Chen, J., Brumbaugh, J., Rigollet, P., Hochedlinger, K., Jaenisch, R., Regev, A., and Lander, E. S. Optimal-Transport Analysis of Single-Cell Gene Expression Identifies Developmental Trajectories in Reprogramming. *Cell*, 176(4):928–943, 2019.
- Schmitz, M. A., Heitz, M., Bonneel, N., Ngolè, F., Coeurjolly, D., Cuturi, M., Peyré, G., and Starck, J.-L. Wasserstein Dictionary Learning: Optimal Transport-Based Unsupervised Nonlinear Dictionary Learning. *SIAM Journal on Imaging Sciences*, 11(1):643–678, jan 2018. doi: 10.1137/17m1140431. URL <https://doi.org/10.1137%2F17m1140431>.

- Serrurier, M., Mamalet, F., Fel, T., Béthune, L., and Boissin, T. On the explainable properties of 1-lipschitz neural networks: An optimal transport perspective, 2023.
- Sinkhorn, R. and Knopp, P. Concerning nonnegative Matrices and doubly stochastic Matrices. *Pacific Journal of Mathematics*, 21(2), 1967.
- Sohl-Dickstein, J., Weiss, E., Maheswaranathan, N., and Ganguli, S. Deep Unsupervised Learning using Nonequilibrium Thermodynamics. In Bach, F. and Blei, D. (eds.), *Proceedings of the 32nd International Conference on Machine Learning*, volume 37 of *Proceedings of Machine Learning Research*, pp. 2256–2265, Lille, France, 07–09 Jul 2015. PMLR. URL <https://proceedings.mlr.press/v37/sohl-dickstein15.html>.
- Song, Y. and Ermon, S. Generative Modeling by Estimating Gradients of the Data Distribution. In Wallach, H., Larochelle, H., Beygelzimer, A., d'Alché-Buc, F., Fox, E., and Garnett, R. (eds.), *Advances in Neural Information Processing Systems*, volume 32. Curran Associates, Inc., 2019. URL <https://proceedings.neurips.cc/paper/2019/file/3001ef257407d5a371a96dcd947c7d93-Paper.pdf>.
- Thornton, J. and Cuturi, M. Rethinking Initialization of the Sinkhorn Algorithm, 2022. URL <https://arxiv.org/abs/2206.07630>.
- Uscidda, T. and Cuturi, M. The monge gap: A regularizer to learn all transport maps, 2023.
- Villani, C. *Optimal Transport Old and New*. Springer, 2009.
- Wang, K., Gou, C., Duan, Y., Lin, Y., Zheng, X., and Wang, F.-Y. Generative adversarial networks: introduction and outlook. *IEEE/CAA Journal of Automatica Sinica*, 4(4): 588–598, 2017. doi: 10.1109/JAS.2017.7510583.
- Zhang, C., Cai, Y., Lin, G., and Shen, C. DeepEMD: Few-Shot Image Classification With Differentiable Earth Mover’s Distance and Structured Classifiers. In *2020 IEEE/CVF Conference on Computer Vision and Pattern Recognition (CVPR)*, pp. 12200–12210, 2020. doi: 10.1109/CVPR42600.2020.01222.

A. Proofs

Proof of Theorem 4.1.

Proof. Since the Lipschitz constant of a composition of functions is bounded by the product of the Lipschitz constants of the components, and similarly, the Lipschitz constant of a sum of Lipschitz functions is bounded by the sum of the Lipschitz constants of the components, we have

$$\text{Lip}(q) \leq \text{Lip}(\text{ReLU})(L + \lambda) = L + \lambda.$$

Now, since we are only interested in images $\mathbf{x} \in \mathbb{R}_{\geq 0}^k$, in the following we can without loss of generality assume that q is of the form $q(\mathbf{z}) = \lambda \mathbf{z} + \text{net}_\theta(\mathbf{z})$.

From Theorem 1 in (Behrmann et al., 2019), it follows that q is invertible, and Lemma 2 therein implies

$$\text{Lip}(q^{-1}) \leq \frac{1}{\lambda - L}.$$

The Lipschitz continuity of q^{-1} implies that for any $\mathbf{h}, \mathbf{z} \in \mathbb{R}^k$ with $\mathbf{h} \neq 0$, we have

$$\|\nabla q(\mathbf{z})\mathbf{h}\| = \lim_{t \rightarrow 0} \left\| \frac{q(\mathbf{z} + t\mathbf{h}) - q(\mathbf{z})}{t} \right\| \geq \frac{1}{\text{Lip}(q^{-1})} \lim_{t \rightarrow 0} \left\| \frac{q^{-1}(q(\mathbf{z} + t\mathbf{h})) - q^{-1}(q(\mathbf{z}))}{t} \right\| = \frac{1}{\text{Lip}(q^{-1})} \|\mathbf{h}\| > 0,$$

which shows that ∇q is invertible everywhere. Hence, by the inverse function theorem, we get

$$\nabla q^{-1}(\mathbf{x}) = \nabla q^{-1}(q(q^{-1}(\mathbf{x}))) = (\nabla q(q^{-1}(\mathbf{x})))^{-1}.$$

Furthermore, similar to above, we have

$$\|\nabla q(\mathbf{z})\mathbf{e}_i\| = \lim_{t \rightarrow 0} \left\| \frac{q(\mathbf{z} + t\mathbf{e}_i) - q(\mathbf{z})}{t} \right\| \leq \text{Lip}(q) \lim_{t \rightarrow 0} \left\| \frac{\mathbf{z} + t\mathbf{e}_i - \mathbf{z}}{t} \right\| \leq L + \lambda,$$

where \mathbf{e}_i is the i^{th} unit vector. Hence, we get from Hadamard's inequality that

$$|\det \nabla q(\mathbf{z})| \leq \prod_i \|\nabla q(\mathbf{z})\mathbf{e}_i\| \leq \prod_i (L + \lambda) = (L + \lambda)^k.$$

Putting everything together, by change of variables, we get

$$\begin{aligned} \rho_{q\# \rho_{\mathbf{z}}}(\mathbf{x}) &= \rho_{\mathbf{z}}(q^{-1}(\mathbf{x})) |\det \nabla q^{-1}(\mathbf{x})| = \rho_{\mathbf{z}}(q^{-1}(\mathbf{x})) |\det \nabla q(q^{-1}(\mathbf{x}))|^{-1} \\ &\geq \rho_{\mathbf{z}}(q^{-1}(\mathbf{x})) \frac{1}{(L + \lambda)^k} = \frac{1}{(L + \lambda)^k} \mathcal{N}(q^{-1}(\mathbf{x}) | 0, I). \end{aligned}$$

□

Proof of Proposition 4.3.

Proof. A well-known fact about the Hilbert metric is that positive matrices (in our case, the Gibb's kernel K) act as strict contractions on positive vectors with respect to the Hilbert metric (cf. Theorem 4.1 in (Peyré & Cuturi, 2019)). More precisely, we have

$$d_H(K\mathbf{v}, K\mathbf{v}') \leq \lambda(K) d_H(\mathbf{v}, \mathbf{v}')$$

for any positive vectors $\mathbf{v}, \mathbf{v}' \in \mathbb{R}^n$, where

$$\lambda(K) := \frac{\sqrt{\eta(K)} - 1}{\sqrt{\eta(K)} + 1}, \quad \eta(K) := \max_{i,j,k,l} \frac{K_{ik}K_{jl}}{K_{jk}K_{il}}.$$

The same inequality also holds for K^\top in place of K . Note that by definition, $\eta(K) \geq 1$, hence $0 < \lambda(K) < 1$. Now consider a starting vector \mathbf{v}^0 to the Sinkhorn algorithm, and let \mathbf{v}^l denote the l^{th} iterate of the vector. Denote by \mathbf{v}^* the limit $\lim_{l \rightarrow \infty} \mathbf{v}^l$ of the algorithm. Then (letting $'//'$ denote element-wise division):

$$\begin{aligned}
 d_H(\mathbf{v}^{l+1}, \mathbf{v}^*) &= d_H(\boldsymbol{\nu}/K^\top \mathbf{u}^{l+1}, \boldsymbol{\nu}/K^\top \mathbf{u}^*) \\
 &= d_H(K^\top \mathbf{u}^{l+1}, K^\top \mathbf{u}^*) \\
 &\leq \lambda(K) d_H(\mathbf{u}^{l+1}, \mathbf{u}^*) \\
 &= \lambda(K) d_H(\boldsymbol{\mu}/K \mathbf{v}^l, \boldsymbol{\mu}/K \mathbf{v}^*) \\
 &= \lambda(K) d_H(K \mathbf{v}^l, K \mathbf{v}^*) \\
 &\leq \lambda(K)^2 d_H(\mathbf{v}^l, \mathbf{v}^*),
 \end{aligned}$$

where we used the Hilbert metric inequality twice, once on K and once on K^\top . Iteratively applying this inequality and translating into log-space notation, this gives us

$$L_H(\mathbf{g}_\tau, \mathbf{g}^*) \leq \lambda(K)^{2k} L_H(\mathbf{g}, \mathbf{g}^*).$$

Hence, by triangle inequality,

$$L_H(\mathbf{g}, \mathbf{g}^*) \leq L_H(\mathbf{g}, \mathbf{g}_\tau) + L_H(\mathbf{g}_\tau, \mathbf{g}^*) \leq L_H(\mathbf{g}, \mathbf{g}_\tau) + \lambda(K)^{2k} L_H(\mathbf{g}, \mathbf{g}^*),$$

which gives us

$$L_H(\mathbf{g}, \mathbf{g}^*) \leq \frac{1}{1 - \lambda(K)^{2k}} L_H(\mathbf{g}_\tau, \mathbf{g}) =: c(K, k) L_H(\mathbf{g}_\tau, \mathbf{g})$$

as desired. □

B. Training Details

Generator. The generator is of the form

$$(\mu, \nu) = q_{\theta}(z) = \text{Renorm}(\text{ReLU}(\text{net}_{\theta}(z) + \lambda T(z)) + c),$$

where we set $\lambda = 1.0$, $c = 1e-2$, and z is of dimension $2 \cdot 14 \cdot 14 = 2 \cdot 196$. The network net_{θ} is a three-layer fully connected network, where the first layer has $2 \cdot 196$ -dimensional in- and $4 \cdot 784$ -dimensional output, the second layer has $4 \cdot 784$ -dimensional in- and output, and the last layer has $4 \cdot 784$ -dimensional in- and $2 \cdot 784$ -dimensional output. The first two layers contain ELU activations and batch normalizations, while the last layer has only sigmoid activations.

We will now describe how one can bound the Lipschitz constant of the generator. Since $\lambda = 1.0$, we need to make sure that the Lipschitz constant of net_{θ} is smaller than 1 in order for theorem 4.1 to be applicable. Since the Lipschitz constant of a composition of functions is bounded by the product of the Lipschitz constants of each component function, this means we have to bound the product of the Lipschitz constants of components of net_{θ} . ELU is Lipschitz continuous with constant 1, whereas sigmoid’s Lipschitz constant is 0.25. Furthermore, for a batch normalization layer BN, we have

$$\|\text{BN}(x) - \text{BN}(y)\| = \left\| \frac{x - \mu}{\sigma} - \frac{y - \mu}{\sigma} \right\| = \frac{1}{\sigma} \|x - y\|,$$

where μ and σ denote the empirical mean and standard deviation of the batch. Since we draw our data from a standard normal Gaussian, we have $\mathbb{E}[\sigma] = 1$, i.e. in expectation, the batch normalization layer is Lipschitz with constant 1. Hence, all that remains is to bound the product of Lipschitz constants of the three linear layers by (any number smaller than) 4 (because the constant of sigmoid is 0.25, this will ensure that the network has a Lipschitz constant smaller than 1), for which it suffices to bound the operator norms of the weight matrix of each layer. In practice, these can be approximated with the power method as in (Gouk et al., 2020) to find a lower bound on the Lipschitz constant of each linear layer, and these bounds can be used to add a soft constraint to the loss. Empirically, this suffices to bound the Lipschitz constant of the generator. Alternatively, one can use a hard constraint as outlined in (Behrmann et al., 2019). However, empirically, this proved detrimental to training, hence we did *not* control the Lipschitz constant during our training. Yet, theorem 4.1 is still of value, as it goes to show that our algorithm’s performance is not bottlenecked by the generator’s inability to generalize. We leave properly enforcing the Lipschitz constraint for future research.

Approximator. The approximator is similar to the network in the generator; a three-layer fully connected network, where the first layer has $2 \cdot 784$ -dimensional in- and $4 \cdot 784$ -dimensional output, the second layer has $4 \cdot 784$ -dimensional in- and output, and the last layer has $4 \cdot 784$ -dimensional in- and 784 -dimensional output. The first two layers contain ELU activations and batch normalizations, while the last layer has neither.

Hyperparameters. We train and test the algorithm on 28×28 -dimensional images, i.e. 784-dimensional distributions. In all experiments, we set $\varepsilon = 0.01$. We use the squared euclidean distance in the unit square as the cost function for our experiments; however, other cost functions could also be considered. Our choice yields the entropic approximation of the squared Wasserstein-2 distance as the optimal transport cost. The learning rate for the generator and approximator is set to 0.25 initially. The generator’s learning rate is left unchanged but we decrease the approximator’s learning rate as follows:

$$\alpha_i \leftarrow 0.99996 \cdot \alpha_{i-1}.$$

The batches for the parameter updates of both networks are of size 500. We use $k = 10$ Sinkhorn updates for the target creation in the training algorithm.

Code. All code used for experiments is available at https://github.com/ingitom99/learn_sink.

C. Additional Material

In order to illustrate the behaviour of the generator over the course of training, we trained it for three times our normal training time, i.e. on 60.000.000 samples, with a skip connection of only 0.5 in order to accentuate the effects of the learned network in the training images. Figure 9 shows the generator’s images over the course of training. As can be seen from the images, the generator behaves very differently at different stages of training. Early on, it prioritizes larger batches of mass at similar locations for μ and ν , while later on, it first starts to move these batches of mass to different locations, before starting to place mass more sparsely. These sparse spots of mass appear both at similar as well as very dissimilar positions across μ and ν . This shows that the generator explores very diverse regions in the space of probability measures over the course of training, in order to generalize as well as possible.

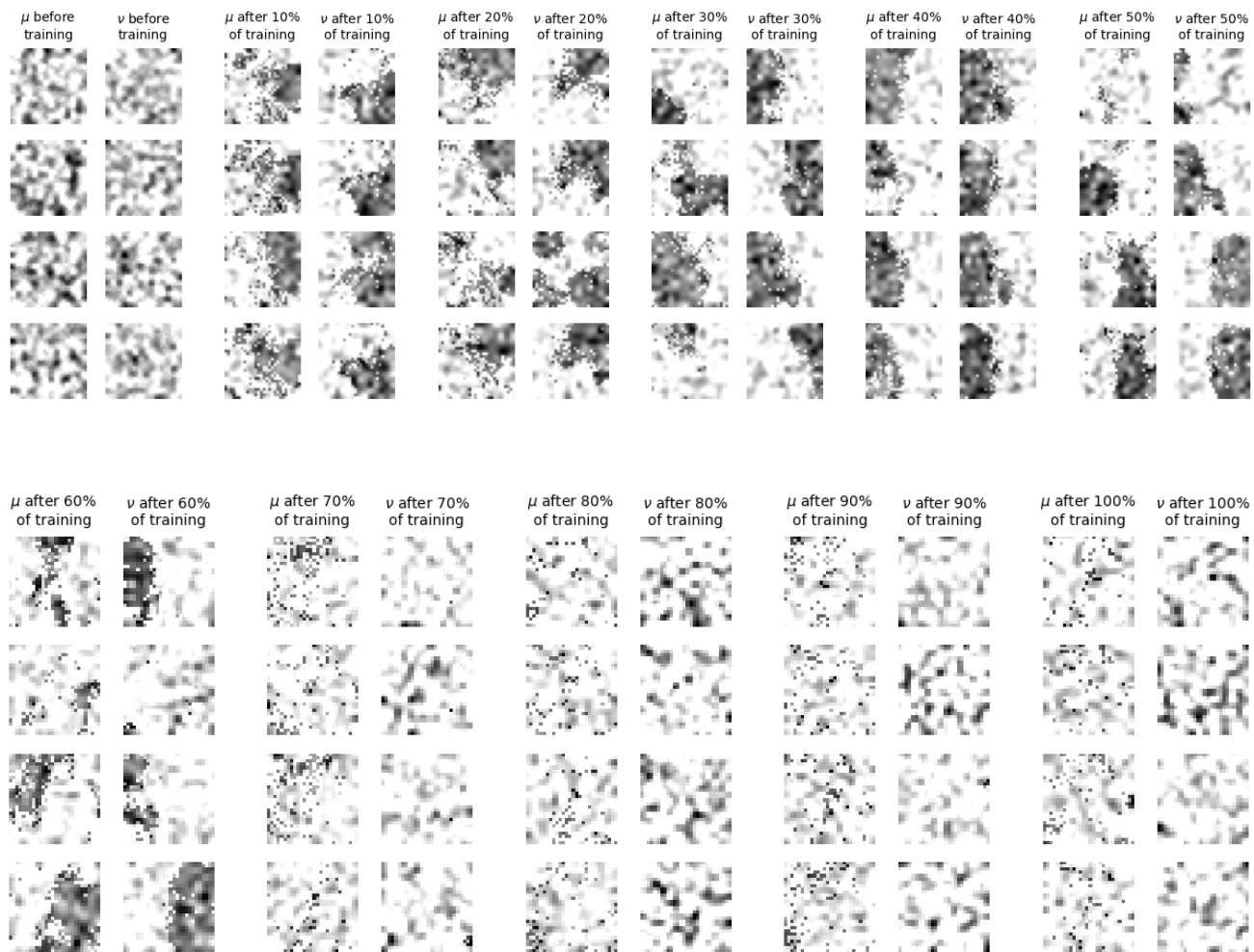


Figure 9. Generated pairs of training samples (darker=more mass).